



# Investigating the physical-chemical effects of reduced graphene oxide-covered manganese oxide on ammonium-ion batteries

Huaxia Chen<sup>a,\*</sup>, Haixin He<sup>a</sup>, Bomiao Wang<sup>a</sup>, Leiyun Han<sup>a</sup>, Jian Ma<sup>a</sup>, Dianpeng Sui<sup>b</sup>, Chongtai Wang<sup>a</sup>, Yingjie Hua<sup>a,\*</sup>

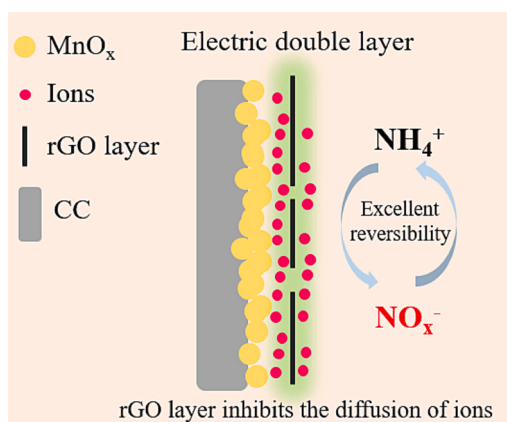
<sup>a</sup> School of Chemistry and Chemical Engineering of Hainan Normal University, Key Laboratory of Electrochemical Energy Storage and Energy Conversion of Hainan Province, Key Laboratory of Electrochemical Energy Storage and Light Energy Conversion Materials of Haikou City, Haikou 571158, China

<sup>b</sup> Department of Chemistry, College of Science, Northeastern University, Shenyang 110819, China.

## HIGHLIGHTS

- Reduced graphene oxide cover on the surface of  $\text{MnO}_x$  to improve the performance of  $\text{MnO}_x$  for ammonium-ion batteries.
- Reduced graphene oxide as blocking layers to inhibit the diffusion of  $\text{Mn}^{2+}$  and  $\text{NO}_x^-$  from the surface of  $\text{MnO}_x$  to electrolyte.
- Investigating the electrochemical effects of reduced graphene oxide layers on  $\text{NH}_4^+$  in electrolyte.

## GRAPHICAL ABSTRACT



## ARTICLE INFO

### Keywords:

Electrochemical coverage  
Reduced graphene oxide  
 $\text{MnO}_x$   
Aqueous ammonium-ion batteries

## ABSTRACT

Aqueous ammonium-ion batteries have attracted more attentions. Electrodeposited manganese oxide ( $\text{MnO}_x$ ) electrodes stand out electrochemical behaviors for storing  $\text{NH}_4^+$ . However, the unsatisfied conductivity and dissolution of  $\text{MnO}_x$  impede electrochemical properties of  $\text{MnO}_x$  for applying in ammonium-ion batteries. In this work, electrochemical coverage of reduced graphene oxide (rGO) layers on  $\text{MnO}_x$  was carried out to improve the properties of  $\text{MnO}_x$  as a positive electrode of ammonium-ion batteries. The improvements are attributed to three functions of rGO additives to engage as conductive layers (fast electron transportation), blocking layers (inhibition of  $\text{Mn}^{2+}$  diffusion) and capacitive behaviors (adsorption of  $\text{Mn}^{2+}$  and  $\text{NO}_x^-$ ), which makes sure the excellent rate capability ( $109 \text{ mAh g}^{-1}$  at  $5 \text{ A g}^{-1}$ ) and cycling stability (92.6% after 1000 cycles) of  $\text{rGO}_{60}/\text{MnO}_x$ . In addition, we also studied the redox of  $\text{NH}_4^+$  on rGO layers to investigate the stability of electrolyte, and the redox of  $\text{NH}_4^+$  on rGO layers is highly reversible and low active, which implies that the rGO is suitable to be a

\* Corresponding authors.

E-mail addresses: [chenhx@hainnu.edu.cn](mailto:chenhx@hainnu.edu.cn) (H. Chen), [521000hua282@sina.com](mailto:521000hua282@sina.com) (Y. Hua).

<https://doi.org/10.1016/j.apenergy.2023.122067>

Received 14 August 2023; Received in revised form 17 September 2023; Accepted 30 September 2023

Available online 11 October 2023

0306-2619/© 2023 Elsevier Ltd. All rights reserved.

functionalized component for improving the properties of  $\text{MnO}_x$  to apply in ammonium-ion batteries. This work provides a new thought to design electrodes with comprehensive strategies for ammonium-ion batteries.

## 1. Introduction

Aqueous rechargeable batteries have many superior advantages of low cost of the electrolyte and manufacture, inherent safety and environmental friendliness compared with nonaqueous battery using organic electrolyte. Sodium ( $\text{Na}^+$ ) [1], potassium ( $\text{K}^+$ ) [2], magnesium ( $\text{Mg}^{2+}$ ) [3], calcium ( $\text{Ca}^{2+}$ ) [4], zinc ( $\text{Zn}^{2+}$ ) [5–7] and aluminum ( $\text{Al}^{3+}$ ) [8] can be charge carriers being stored in appropriate host electrodes in aqueous electrolyte. Additionally, ammonium ion ( $\text{NH}_4^+$ ) can also be charge carriers being stored in host electrodes in aqueous electrolyte through intercalation [9] or H-bond [10].  $\text{NH}_4^+$  as charge carriers stand out due to its abundant resources (low cost), small hydrated ionic size (3.31 Å) (fast diffusion) and low molar mass (18 g mol<sup>-1</sup>) (high gravimetric specific capacity) [11].

For electrolytes, ammonium salt dissolved in water is directly engaged as electrolyte, such as  $\text{NH}_4\text{Ac}$ ,  $(\text{NH}_4)_2\text{SO}_4$  and  $\text{NH}_4\text{NO}_3$ . For electrode materials, many attempts have been proposed. For example, the pioneering work on Prussian blue analogues (PBAs) in 2012 [12], subsequently  $\text{Ti}_3\text{C}_2$  MXene [13], organic solids (polyaniline [14] etc.) and metal oxide (titanic acid [15],  $\text{V}_2\text{O}_5$  [16],  $\text{MoO}_3$  [17] etc.), which were studied from the aspects of electrochemical performance and storing mechanism of  $\text{NH}_4^+$ . Noteworthy, Song et al. [10] firstly reported in 2021 that  $\text{NH}_4^+$  can be stored in electrodeposited manganese oxide ( $\text{MnO}_x$ ) by the formation of H-bond between  $\text{NH}_4^+$  and the  $\text{MnO}_x$  layers, which delivered a high specific capacity of 176 mAh g<sup>-1</sup>. Besides electrochemical properties, the electrodeposition is a convenient and practical strategy to obtain earth-abundant  $\text{MnO}_x$  electrode materials. However, it is recognized that manganese oxide-based electrode possesses an unsatisfied electrical conductivity compared with some carbon materials with high electrical conductivity such as carbon nanotube and graphene. The unsatisfied electrical conductivity can lead to a low efficiency of the conversions between chemical energy and electric energy during charging/discharging process. Furthermore, many researches emphasized the phenomenon of dissolution of manganese oxide (conversion of high valence Mn into  $\text{Mn}^{2+}$ ) during charging/discharging process in aqueous electrolyte systems [18–20], and the chemical instability of manganese oxide induces the electrochemical instability of manganese oxide during long-term cyclic process. Additionally, according to E–pH diagrams of nitrogen element,  $\text{NH}_4^+$  can be electrochemically oxidized to  $\text{NO}_2^-$  and  $\text{NO}_3^-$  in positive potential regions [21,22], and the potential instability of electrolyte needs to be carefully considered in the process of designing electrodes for practical applications of ammonium-ion batteries. Except for above problems, the low voltage of many aqueous ammonium-ion batteries is also a pivotal quandary for further applications, which should be seriously considered for designing aqueous ammonium-ion batteries in the future [23].

Integrated considerations of poor conductivity of manganese oxide, dissolution of manganese oxide and the oxidation of  $\text{NH}_4^+$ , adopting tight

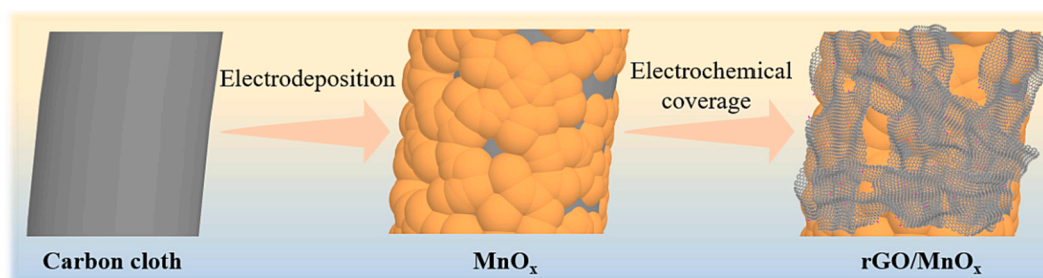
and incomplete coverage of reduced graphene oxide (rGO) layers on  $\text{MnO}_x$  may be a feasible strategy to improve the performance of  $\text{MnO}_x$  for applying  $\text{MnO}_x$  in ammonium-ion batteries. rGO layers could improve the conductivity of whole electrode, which raises the effective utilization of  $\text{MnO}_x$  resulting in improved rate capability of  $\text{MnO}_x$ -based electrode. The existence of narrow space between rGO layers and  $\text{MnO}_x$  could restrict the diffusion of  $\text{Mn}^{2+}$  and  $\text{NO}_3^-$  into bulk electrolyte, which guarantees the regenerations of  $\text{MnO}_x$  and  $\text{NH}_4^+$  from  $\text{Mn}^{2+}$  and  $\text{NO}_3^-$  resulting in improved stability of ammonium-ion batteries. Based on above strategy, this work used electrochemical methods to initially electrodeposit the  $\text{MnO}_x$  on carbon cloth, and the rGO layers subsequently covered on the surface of  $\text{MnO}_x$  to fabricate rGO/ $\text{MnO}_x$  electrode to apply in ammonium-ion batteries as illustrated in Scheme 1. The physical-chemical effects of rGO layers on  $\text{MnO}_x$  was investigated through a series of characterizations, electrochemical determinations and systematic analyzations of experimental data.

## 2. Results and discussion

### 2.1. Electrochemical coverage of rGO layers on $\text{MnO}_x$

For synthesis of rGO/ $\text{MnO}_x$ ,  $\text{MnO}_x$  and rGO are successively electrodeposited on carbon cloth. The details can be seen in Supporting Information. The  $\text{Mn}^{2+}$  can be oxidated on carbon cloth, which can reflect on the appearance of strong redox peak of carbon cloth in  $\text{MnAc}_2$  electrolyte as shown in Fig. S1. Aiming to quickly obtain  $\text{MnO}_x$ , the  $\text{MnO}_x$  were electrodeposited on carbon cloth at an anodic current of 20 mA cm<sup>-2</sup> as shown in Fig. 1a, and the morphology of  $\text{MnO}_x$  are sphere with the aggregation of the dense nanoparticles inset of Fig. 1a. According to the reported work [8], the  $\text{MnO}_x$  will undergo a morphological transformation during initial charging/discharging cycles in  $\text{NH}_4\text{Ac}$  electrolyte. Hence, the stable morphology is required to be found, otherwise the rGO layers could break and fall off the  $\text{MnO}_x$  as shown in Fig. S2a and Fig. S2b. It is obvious that the dense nanoparticles grow up after 5 charging/discharging cycles (Fig. 1b), then the aggregated nanoparticles transform into the aggregated slices after 20 charging/discharging cycles (Fig. 1c), finally the size of aggregated slices is unchanged after 40 charging/discharging cycles compared with these after 50 charging/discharging cycles (Fig. 1d). In this case,  $\text{MnO}_x$  after 40 cycles was selected to be stable substrates to electrochemically cover rGO layers.

The electrochemical coverage of rGO layers was operated in a two-electrode cell at a constant current of 1 mA cm<sup>-2</sup> as shown in Fig. 2a. Graphite foil and  $\text{MnO}_x$  on carbon cloth were used as anode and cathode, respectively, and 0.1 mg mL GO with 0.01 M  $\text{Na}_2\text{SO}_4$  was used as electrolyte. To avoid the effect of O content in  $\text{MnO}_x$  on measurement of O content in graphene oxide, the carbon cloth was directly covered by graphene oxide to investigate the O content of graphene oxide (Fig. 2b).



**Scheme 1.** The process of preparing rGO/ $\text{MnO}_x$  on carbon cloth using electrochemical methods.

Fig. 2c and Fig. 2d show the element distributions of C and O. The amount of O in GO (Fig. S3) is decreased after electrochemically covering on carbon cloth (Fig. 2c and Fig. 2d) indicating the reduction of GO during cathodic reactions. The amounts of rGO layers on  $\text{MnO}_x$  is different at electrodeposited time of 60 s, 150 s and 300 s. It is obvious from the SEM images that rGO layers partially cover on  $\text{MnO}_x$  tightly after 60 s (Fig. 2e). The  $\text{MnO}_x$  was covered by rGO layers, but with a few small holes after 150 s (Fig. 2f). The rGO layers completely cover on  $\text{MnO}_x$  without any holes after 300 s (Fig. 2g). Depending on different coverage times, the rGO/ $\text{MnO}_x$  is denoted as  $\text{rGO}_{60}/\text{MnO}_x$ ,  $\text{rGO}_{150}/\text{MnO}_x$  and  $\text{rGO}_{300}/\text{MnO}_x$ , respectively. XRD patterns of  $\text{MnO}_x$  and  $\text{rGO}_{60}/\text{MnO}_x$  display a similar characteristic peak of carbon cloth indicating the amorphous  $\text{MnO}_x$  on carbon cloth and in  $\text{rGO}_{60}/\text{MnO}_x$  as shown in Fig. 2h. Besides, there is no obvious change in the XPS of Mn  $2p_{1/2}$  of  $\text{MnO}_x$  and  $\text{rGO}_{300}/\text{MnO}_x$  as shown in Fig. 2i, which demonstrates that the valence state of  $\text{MnO}_x$  is not changed after cathodic reactions of covering rGO layers.

## 2.2. Electrochemical performance of $\text{MnO}_x$ and rGO/ $\text{MnO}_x$ in $\text{NH}_4^+$ electrolyte

This section mainly aims to discuss the electrochemical effects of rGO layers on  $\text{MnO}_x$  in  $\text{NH}_4^+$  electrolyte by electrochemical comparisons of  $\text{MnO}_x$ ,  $\text{rGO}_{30}/\text{MnO}_x$ ,  $\text{rGO}_{60}/\text{MnO}_x$ ,  $\text{rGO}_{150}/\text{MnO}_x$  and  $\text{rGO}_{300}/\text{MnO}_x$ . Fig. 3a shows the CV curves of  $\text{MnO}_x$ ,  $\text{rGO}_{30}/\text{MnO}_x$ ,  $\text{rGO}_{60}/\text{MnO}_x$ ,  $\text{rGO}_{150}/\text{MnO}_x$  and  $\text{rGO}_{300}/\text{MnO}_x$ . The CV curve of  $\text{rGO}_{30}/\text{MnO}_x$  shows a similar peak current compared with that of  $\text{MnO}_x$ . This may be related to the less coverage of rGO on  $\text{MnO}_x$  in a short deposition time (30 s), and

the rGO cannot form connected layers to work as conductive layers as shown in Fig. S2c and Fig. S2d. The peak current of rGO/ $\text{MnO}_x$  is higher than that of  $\text{MnO}_x$  indicating that the rGO layers form another channel for electron transportations to the whole  $\text{MnO}_x$  electrode (rGO/ $\text{MnO}_x$ ) during  $\text{NH}_4^+$  intercalation/deintercalation process. Particularly, the coverage of rGO layers could arouse the activity of  $\text{MnO}_x$  far from the carbon cloth and near to rGO layers, which improves the effective utilization of  $\text{MnO}_x$ . Among  $\text{rGO}_{60}/\text{MnO}_x$ ,  $\text{rGO}_{150}/\text{MnO}_x$  and  $\text{rGO}_{300}/\text{MnO}_x$ , the peak currents follow the order of  $\text{rGO}_{60}/\text{MnO}_x > \text{rGO}_{150}/\text{MnO}_x > \text{rGO}_{300}/\text{MnO}_x$ , which can be attributed to the thickness of rGO layers on  $\text{MnO}_x$ . Thick rGO layers leads to less holes on the surface of  $\text{MnO}_x$ , which impedes the diffusions of  $\text{NH}_4^+$  from the bulk electrolyte to the surface of  $\text{MnO}_x$  during electrochemical process. Besides, thick rGO layers results in poorer conductivity of rGO layers, which hinders the electron transportations during electrochemical process. The  $\text{rGO}_{60}/\text{MnO}_x$  delivers highest specific capacity of  $173 \text{ mAh g}^{-1}$  compared with  $\text{MnO}_x$  ( $149 \text{ mAh g}^{-1}$ ),  $\text{rGO}_{30}/\text{MnO}_x$  ( $151 \text{ mAh g}^{-1}$ ),  $\text{rGO}_{150}/\text{MnO}_x$  ( $163 \text{ mAh g}^{-1}$ ) and  $\text{rGO}_{300}/\text{MnO}_x$  ( $155 \text{ mAh g}^{-1}$ ) as shown in Fig. 3b. Through the comparison between the CV and GCD curves, there is no obvious improvement of  $\text{rGO}_{30}/\text{MnO}_x$  compared to  $\text{MnO}_x$ . Hence, the sample of  $\text{rGO}_{30}/\text{MnO}_x$  is ignored in the following discussions. Otherwise,  $\text{rGO}_{60}/\text{MnO}_x$  also presents an improved rate capability as shown in Fig. 3c, and the specific capacity of  $\text{rGO}_{60}/\text{MnO}_x$  decreases from  $173 \text{ mAh g}^{-1}$  ( $0.5 \text{ A g}^{-1}$ ) to  $109 \text{ mAh g}^{-1}$  ( $5 \text{ A g}^{-1}$ ), while the specific capacity of  $\text{MnO}_x$  decreases from  $149 \text{ mAh g}^{-1}$  ( $0.5 \text{ A g}^{-1}$ ) to  $73 \text{ mAh g}^{-1}$  ( $5 \text{ A g}^{-1}$ ).

Cycling stability is an important parameter to evaluate batteries. Fig. 3d shows the cycling stability of  $\text{MnO}_x$  and  $\text{rGO}_{60}/\text{MnO}_x$ . The

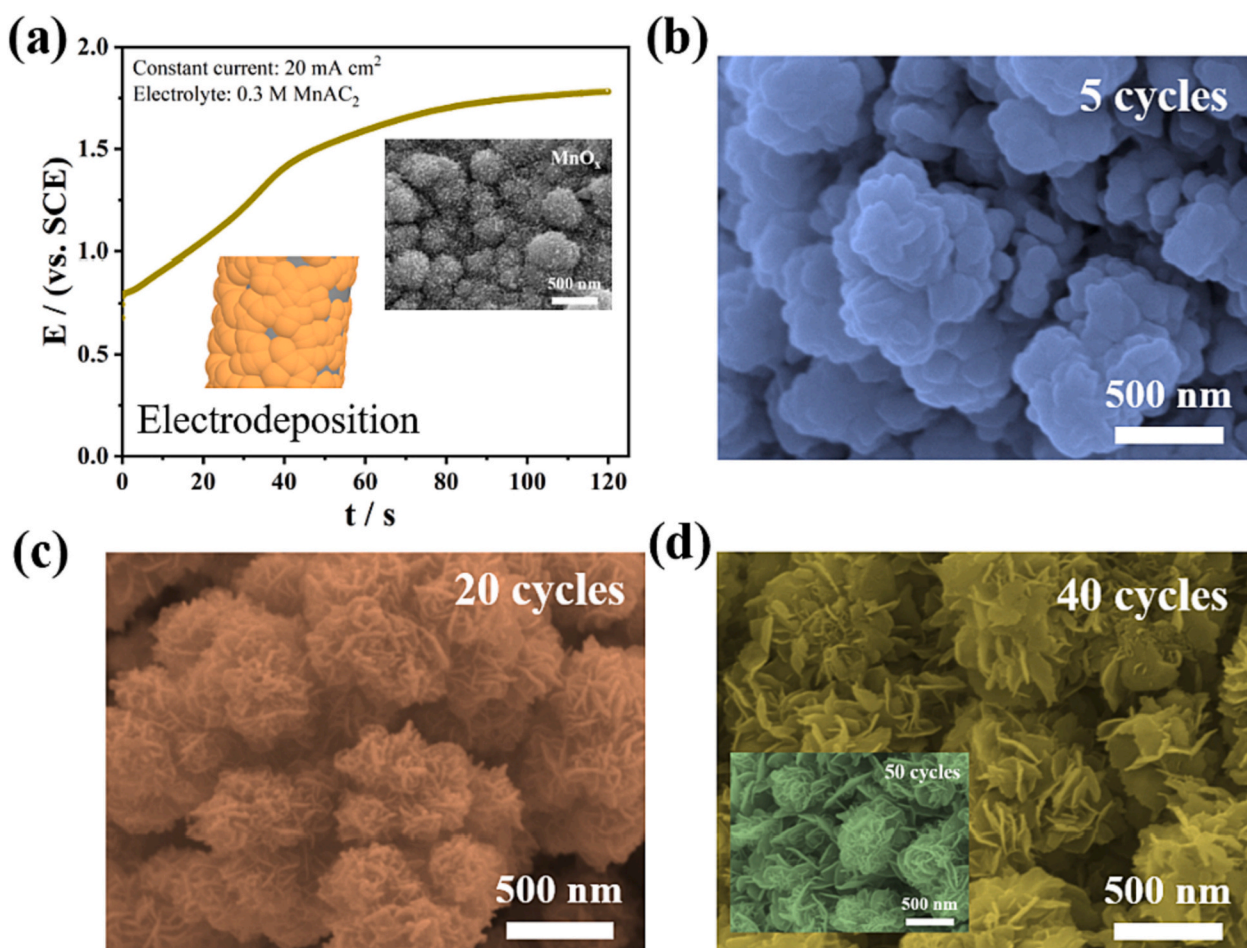


Fig. 1. (a) Electrodeposition of  $\text{MnO}_x$  on carbon cloth at a constant current of  $20 \text{ mA cm}^{-2}$  in a three-electrode system. Inset shows SEM images of  $\text{MnO}_x$ . The SEM images of  $\text{MnO}_x$  after 5 cycles (b), 20 cycles (c) and 40 cycles (d) with inset of 50 cycles in  $0.5 \text{ M NH}_4\text{Ac}$  electrolyte.



specific capacity of  $\text{MnO}_x$  decreased from  $150 \text{ mAh g}^{-1}$  to  $140 \text{ mAh g}^{-1}$  at  $0.5 \text{ A g}^{-1}$  after 100 cycles. Compared with  $\text{MnO}_x$ , the specific capacity of  $\text{rGO}_{60}/\text{MnO}_x$  is almost unchanged (from  $171 \text{ mAh g}^{-1}$  to  $170 \text{ mAh g}^{-1}$ ) after 100 cycles (inset of Fig. 3d). Even at a high current density of  $5 \text{ A g}^{-1}$ , the specific capacity of  $\text{rGO}_{60}/\text{MnO}_x$  decreased from  $108 \text{ mAh g}^{-1}$  to  $100 \text{ mAh g}^{-1}$  (92.6%) as shown in Fig. S4. The cycling stability of  $\text{MnO}_x$  is related to the chemical stability of  $\text{MnO}_x$ . We studied the element in electrolyte using ICP-mass, and the concentration of Mn ions in electrolyte is  $21.02 \text{ mg L}^{-1}$  after 1000 cycles when the  $\text{MnO}_x$  serves as a working electrode as listed in Table 1. However, the concentration of Mn ion in electrolyte is  $15.37 \text{ mg L}^{-1}$  (Equivalent to  $0.39 \text{ mg MnO}$  and  $0.49 \text{ mg MnO}_2$ ) when the  $\text{rGO}_{60}/\text{MnO}_x$  serves as a working electrode, which is lower than  $21.02 \text{ mg L}^{-1}$  (Equivalent to  $0.54 \text{ mg MnO}$  and  $0.66 \text{ mg MnO}_2$ ). The Mn ions in electrolyte probably dissolved from  $\text{MnO}_x$  during charging/discharging process. The rGO could be blocked layers partially inhibiting Mn ion to diffuse into electrolyte far from electrode surface, so the Mn ion has more chances to regenerate  $\text{MnO}_x$  on the surface of  $\text{MnO}_x$ . Hence, the rGO layers indirectly improve the chemical stability of  $\text{MnO}_x$ , which improves cycling stability of  $\text{MnO}_x$ . Moreover, we noticed that the UV-visible spectroscopy of  $\text{NH}_4\text{Ac}$  aqueous shows different absorption peaks after cycling in  $\text{MnO}_x$ - and  $\text{rGO}_{60}/\text{MnO}_x$ -based batteries compared with original  $\text{NH}_4\text{Ac}$  indicating the decomposition of  $\text{NH}_4\text{Ac}$  as shown in Fig. S5a, because the  $\text{NH}_4^+$  could be theoretically oxidized to  $\text{NO}_2^-$  and  $\text{NO}_3^-$  based on the  $E$ -pH diagram of Nitrogen (Fig. S5b). Further, we compared the ion species of electrolyte

between original electrolyte and cycled electrolyte ( $\text{MnO}_x$ - and  $\text{rGO}_{60}/\text{MnO}_x$ -based battery) using Ion Chromatography as listed in Table 1. The  $\text{NO}_2^-$  ( $314.2 \text{ mg L}^{-1}$ ) was detected in electrolyte after 1000 cycles when the  $\text{MnO}_x$  serve as a working electrode. This proves the instability of  $\text{NH}_4^+$  in electrolyte, which can be oxidized into  $\text{NO}_2^-$  by  $\text{MnO}_x$  during long-term cycles. The instability of  $\text{NH}_4^+$  (intercalation/deintercalation agents) may give rise to the instability of electrochemical performance. Similarly, the blocking layers in  $\text{rGO}_{60}/\text{MnO}_x$  could also partially impede the diffusion of  $\text{NO}_2^-$ , which could be probably reduced into  $\text{NH}_4^+$  on the surface of  $\text{MnO}_x$  resulting in less  $\text{NO}_2^-$  formations ( $188.8 \text{ mg L}^{-1}$ ) in the system of  $\text{rGO}_{60}/\text{MnO}_x$  during electrochemical cycles. Besides, the  $\text{NO}_3^-$  cannot be detected by Ion Chromatography owing to less or no  $\text{NO}_3^-$  in electrolyte whose concentration is below the detecting limit of Ion chromatography. Less or no  $\text{NO}_3^-$  indicates that redox couple of  $\text{NO}_3^-/\text{NO}_2^-$  exhibits an excellent reversibility on the surface of electrode. According to above discussions, rGO layers can improve the stability of  $\text{MnO}_x$ -based ammonium-ion batteries through indirect enhancement of chemical stability of  $\text{MnO}_x$  and  $\text{NH}_4^+$ .

Electrochemical impedance spectroscopy was used to further clarify the electrochemical processes of  $\text{MnO}_x$ ,  $\text{rGO}_{60}/\text{MnO}_x$ ,  $\text{rGO}_{150}/\text{MnO}_x$ , and  $\text{rGO}_{300}/\text{MnO}_x$  electrodes. Fig. 4a presents the Nyquist plots of  $\text{MnO}_x$ ,  $\text{rGO}_{60}/\text{MnO}_x$ ,  $\text{rGO}_{150}/\text{MnO}_x$ , and  $\text{rGO}_{300}/\text{MnO}_x$ . It is obvious that the imaginary part of the impedance sharply increases for  $\text{rGO}_{60}/\text{MnO}_x$ ,  $\text{rGO}_{150}/\text{MnO}_x$ , and  $\text{rGO}_{300}/\text{MnO}_x$ . The plot tends to a vertical line characteristic especially for  $\text{rGO}_{60}/\text{MnO}_x$  indicating the capacitive

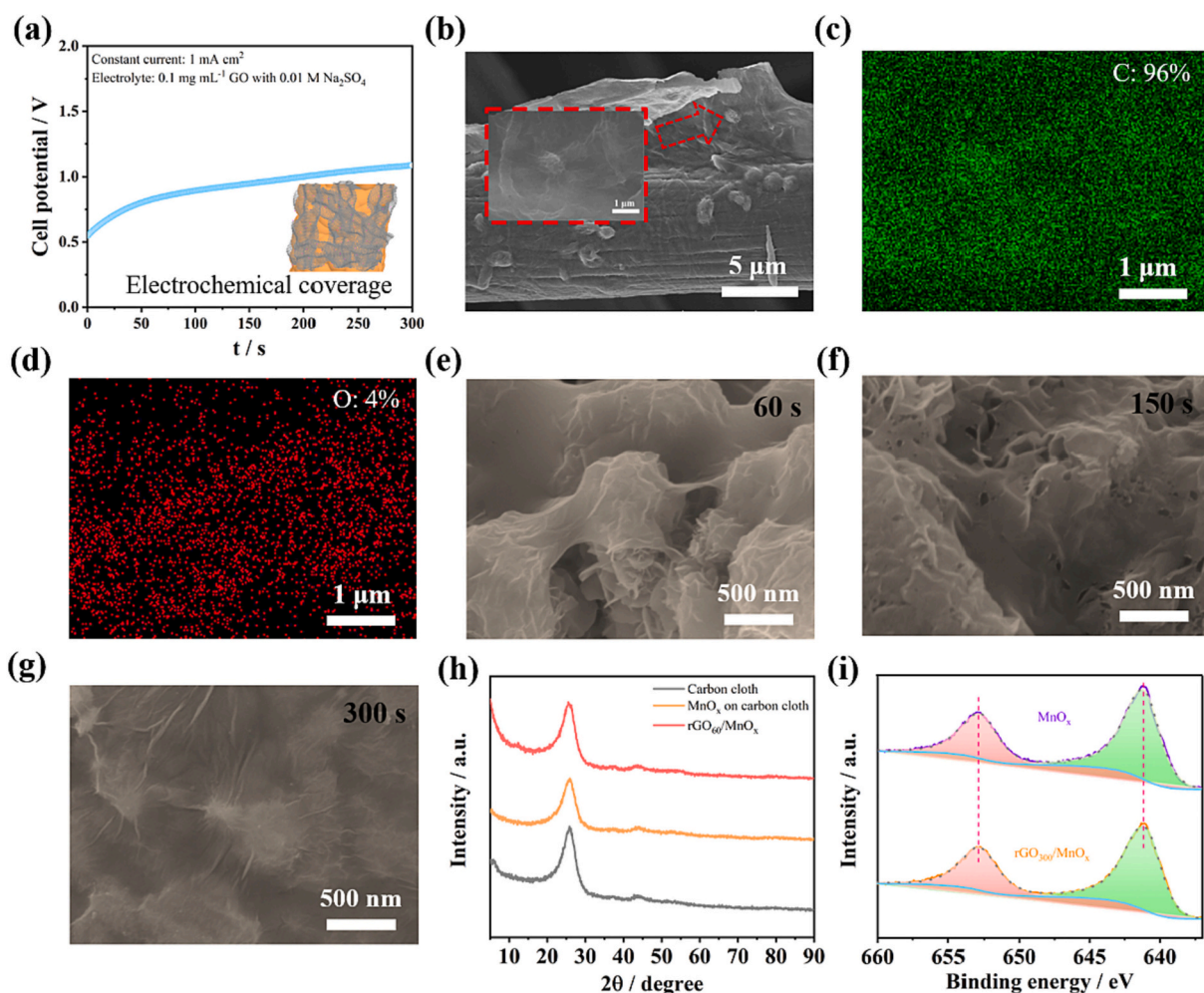


**Fig. 2.** (a) Electrochemical coverage of rGO layers on  $\text{MnO}_x$  at a constant current of  $1 \text{ mA cm}^{-2}$  in a two-electrode cell. The SEM image (b) and element distributions (c and d) of rGO on carbon cloth. The SEM images of  $\text{rGO}_{60}/\text{MnO}_x$  (e),  $\text{rGO}_{150}/\text{MnO}_x$  (f) and  $\text{rGO}_{300}/\text{MnO}_x$  (g). (h) The XRD patterns of carbon cloth,  $\text{MnO}_x$  on carbon cloth and  $\text{rGO}_{60}/\text{MnO}_x$ . (i) XPS Mn  $2p_{1/2}$  spectra of  $\text{MnO}_x$  and  $\text{rGO}_{300}/\text{MnO}_x$ .

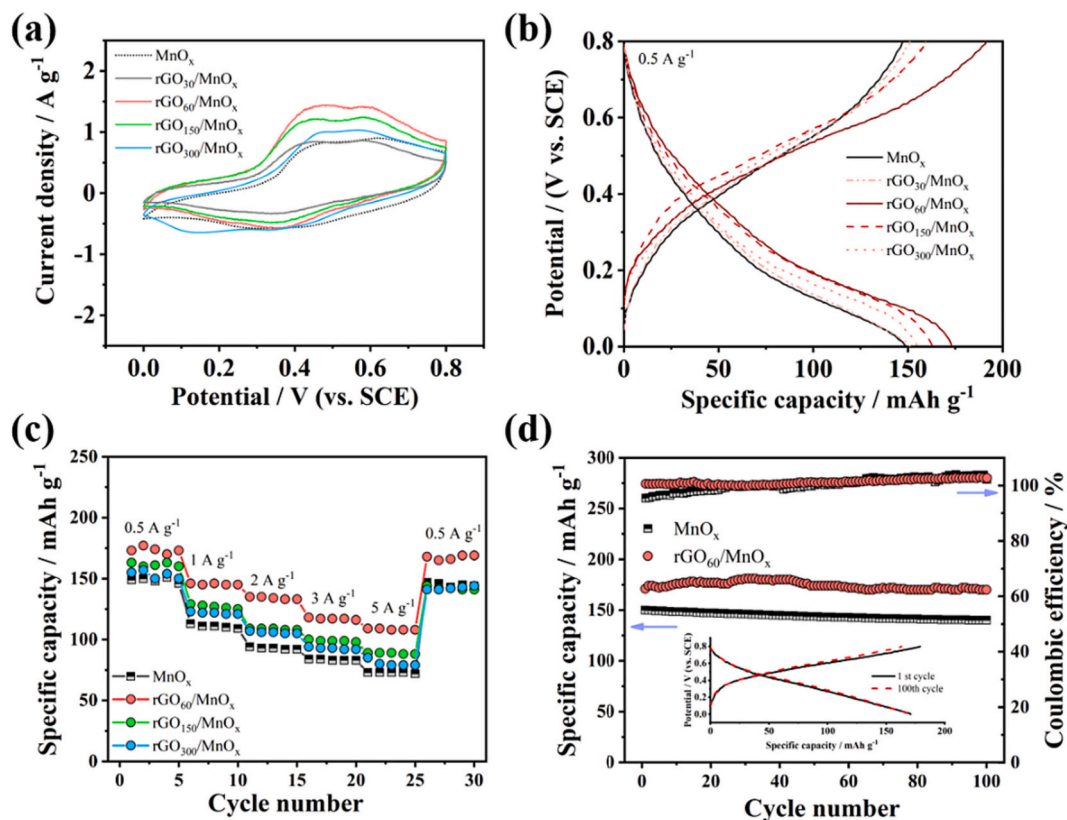


**Fig. 3.** (a) CV curves of  $\text{MnO}_x$ ,  $\text{rGO}_{30}/\text{MnO}_x$ ,  $\text{rGO}_{60}/\text{MnO}_x$ ,  $\text{rGO}_{150}/\text{MnO}_x$  and  $\text{rGO}_{300}/\text{MnO}_x$ . (b) GCD curves of  $\text{MnO}_x$ ,  $\text{rGO}_{30}/\text{MnO}_x$ ,  $\text{rGO}_{60}/\text{MnO}_x$ ,  $\text{rGO}_{150}/\text{MnO}_x$  and  $\text{rGO}_{300}/\text{MnO}_x$ . (c) Rate capability of  $\text{MnO}_x$ ,  $\text{rGO}_{60}/\text{MnO}_x$ ,  $\text{rGO}_{150}/\text{MnO}_x$  and  $\text{rGO}_{300}/\text{MnO}_x$  at the current density of  $0.5 \text{ A g}^{-1}$ . (d) Cycling stability and coulombic efficiency of  $\text{MnO}_x$  and  $\text{rGO}_{60}/\text{MnO}_x$  at the current density of  $0.5 \text{ A g}^{-1}$ .

**Table 1**

The concentration of species in initial electrolyte and electrolyte after 1000 cycles at  $5 \text{ A g}^{-1}$ .

Species	Concentration of ion species in electrolyte ( $\text{mg L}^{-1}$ )		
	Initial electrolyte	In $\text{MnO}_x$	In $\text{rGO}_{60}/\text{MnO}_x$
$\text{Mn}^{2+}$	/	21.02	15.37
$\text{NH}_4^+$	1068	990.5	996.9
$\text{NO}_2^-$	/	314.2	188.8
$\text{NO}_3^-$	/	/	/

The concentration of  $\text{Mn}^{2+}$  was measured by ICP-mass; The concentrations of  $\text{NH}_4^+$ ,  $\text{NO}_2^-$  and  $\text{NO}_3^-$  were measured by Ion Chromatography.

behavior of  $\text{rGO}_{60}/\text{MnO}_x$  electrode as the equation shown in Fig. 4a. Identically, the real part of capacitance ( $C'$ ) corresponds to the capacitance of the electrode at low frequency value [24]. Fig. 4b shows a higher capacitance of  $\text{rGO}_{60}/\text{MnO}_x$  compared with  $\text{rGO}_{150}/\text{MnO}_x$ ,  $\text{rGO}_{300}/\text{MnO}_x$  and  $\text{MnO}_x$ . The capacitance of  $\text{rGO}_{60}/\text{MnO}_x$ ,  $\text{rGO}_{150}/\text{MnO}_x$  and  $\text{rGO}_{300}/\text{MnO}_x$  is gradually decreased as shown in Fig. 4b. This could be related to the thickness of rGO layers. Thick rGO layers exhibit the properties of small specific surface area and low conductivity because of the restack of rGO sheets. It is also reflected from the impedance (Bode plot) of  $\text{MnO}_x$ ,  $\text{rGO}_{60}/\text{MnO}_x$ ,  $\text{rGO}_{150}/\text{MnO}_x$ , and  $\text{rGO}_{300}/\text{MnO}_x$  as shown in Fig. 4c. Bode plot shows that the impedance value of  $\text{rGO}_{60}/\text{MnO}_x$  is lower than that of  $\text{MnO}_x$  [25]. As discussed above, rGO layers can be conductive components during charging/discharging process. At the same time, rGO layers can also provide extra capacitance. Though the capacitance of rGO layers is low, the electric double layer could electrochemically adsorb ions such as  $\text{Mn}^{2+}$  and  $\text{NO}_x^-$  (a probable part of the electric double layer), which forces these ions diffuse into electrolyte not far from electrode surface. The electric

double layer formed by rGO layers can be divided into inner layer and outer layer as shown in Fig. 4d. A narrow space is constructed between inner layer and  $\text{MnO}_x$  surface, which is the main region to electrochemically adsorb  $\text{Mn}^{2+}$  and  $\text{NO}_x^-$ . Outer layer could also electrochemically adsorb  $\text{Mn}^{2+}$  and  $\text{NO}_x^-$  which are not far from the outer surface of the rGO layers. This part of  $\text{Mn}^{2+}$  and  $\text{NO}_x^-$  in the bulk electrolyte originates from the narrow space forming by the surface of  $\text{MnO}_x$  and the inner surface of rGO. In a conclusion, the electric double layer formed by rGO layers and ions contribute another part of cycling stability.

### 2.3. The effects of rGO layers on $\text{NH}_4^+$

According to the E-pH diagram of Nitrogen, the  $\text{NH}_4^+$  is instable in positive potentials. Through a simulative calculation of  $0.5 \text{ M NH}_4\text{Ac}$  (aqueous solution) using Visual MINTEQ (Table S1), there are chemical equilibriums between  $\text{NH}_4^+$  and  $\text{NH}_3$ , and  $\text{NH}_3$  could undergo a series of electrochemical oxidations [26–28]. Therefore, the rGO layers serving as additive components should be investigated (whether rGO can catalyze oxidation of  $\text{NH}_4^+$ ) to make sure the rationality of applying rGO in ammonium-ion batteries. Fig. 5 shows the CV curves of carbon cloth and rGO layers on carbon cloth in  $0.5 \text{ M NH}_4\text{Ac}$  in the working potential from 0 to  $0.8 \text{ V}$ . The CV curve of rGO shows two complete and reversible peaks which may be attributed to the formations of  $\text{NO}$  and  $\text{NO}_2^-$ , respectively. When the potential reaches to  $0.8 \text{ V}$  of rGO layers-covered electrode, there is an incomplete oxidation peak possibly attributing to the formation of  $\text{NO}_3^-$  indicating the low degree oxidation of  $\text{NH}_4^+$  to  $\text{NO}_3^-$ . This may be the reasons for hardly detecting  $\text{NO}_3^-$  in the electrolyte using IC after 1000 cycles. The reversible peaks with low current demonstrate that rGO layers can catalyze the redox of  $\text{NH}_4^+$  in a low degree. However, due to the enhanced inhibition of rGO layers, the  $\text{NO}_x^-$

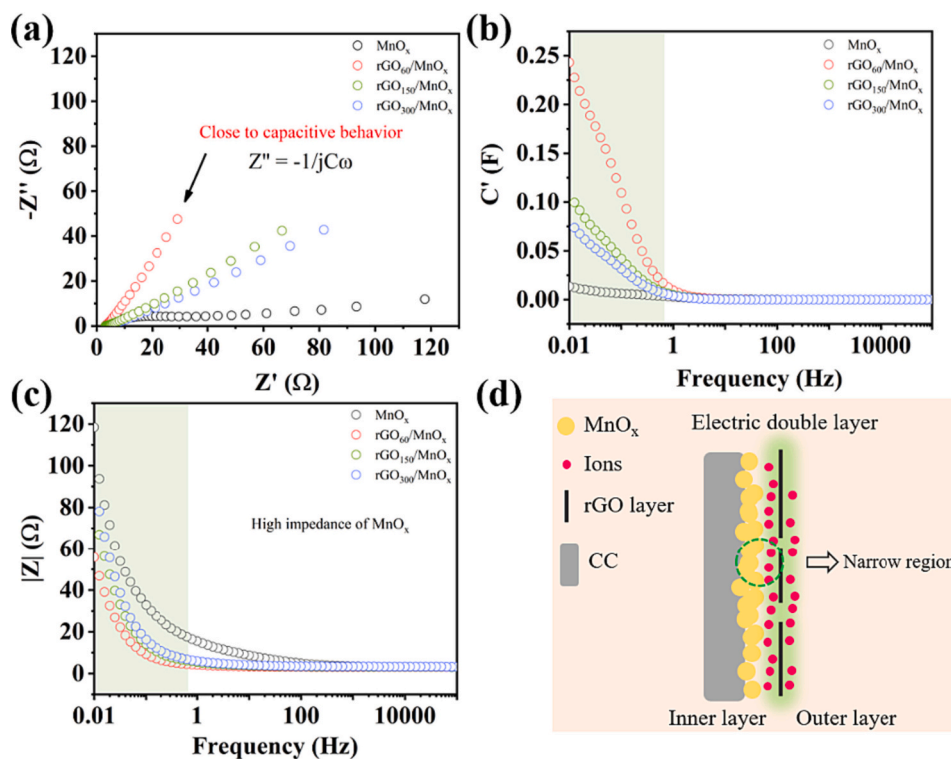


Fig. 4. (a) Nyquist plots of MnO<sub>x</sub>, rGO<sub>60</sub>/MnO<sub>x</sub>, rGO<sub>150</sub>/MnO<sub>x</sub> and rGO<sub>300</sub>/MnO<sub>x</sub>. (b) The real part vs. frequency for MnO<sub>x</sub>, rGO<sub>60</sub>/MnO<sub>x</sub>, rGO<sub>150</sub>/MnO<sub>x</sub> and rGO<sub>300</sub>/MnO<sub>x</sub>. (c) Bode plots of MnO<sub>x</sub>, rGO<sub>60</sub>/MnO<sub>x</sub>, rGO<sub>150</sub>/MnO<sub>x</sub> and rGO<sub>300</sub>/MnO<sub>x</sub>. (d) The schematic picture for explaining the narrow region originating from electric double layer of rGO layer.

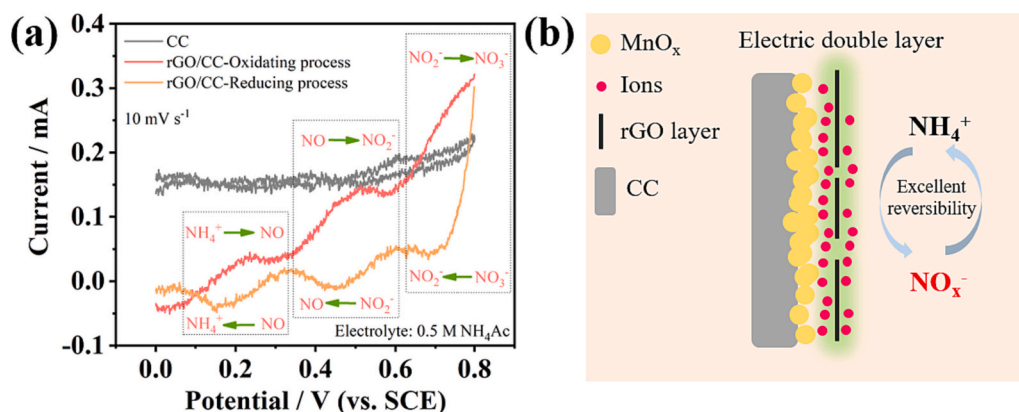


Fig. 5. (a) The CV curves of carbon cloth and rGO/CC in 0.5 M NH<sub>4</sub>Ac. (b) The schematic picture for electrochemical reactions of NH<sub>4</sub><sup>+</sup> on rGO layers.

could exist near to the rGO layers for the regeneration of NH<sub>4</sub><sup>+</sup> as shown in Fig. 5b, which guarantees the cycling stability of ammonium-ion batteries. Hence, the rGO layers can be additive components for constructing the electrode of ammonium-ion batteries.

### 3. Conclusions

rGO layers were electrochemically cover on the surface of MnO<sub>x</sub>, which can improve the electrochemical performance of MnO<sub>x</sub> applied in ammonium-ion batteries. The rGO<sub>60</sub>/MnO<sub>x</sub> shows an enhanced rate capability (109 mAh g<sup>-1</sup> at 5 A g<sup>-1</sup>) and cycling stability (92.6% after 1000 cycles). The improved performance of ammonium-ion batteries from rGO layers can be summarized as three aspects. First, the rGO layers can be conductive components to facilitate electrons transportation to whole MnO<sub>x</sub> electrodes, which leads to an optimized rate capability of rGO<sub>60</sub>/MnO<sub>x</sub>. Second, the rGO layers can be blocking layers

to inhibit the Mn<sup>2+</sup> and NO<sub>x</sub><sup>-</sup> diffuse far from electrode, which leads to an optimized cycling stability of rGO<sub>60</sub>/MnO<sub>x</sub>. Based on the function of blocking layers, the capacitive behavior of rGO layers also boost the blocking functions by electrochemical adsorptions of Mn<sup>2+</sup> and NO<sub>x</sub><sup>-</sup>. In addition, as a component of rGO<sub>60</sub>/MnO<sub>x</sub>, the redox of NH<sub>4</sub><sup>+</sup> on rGO layers show high reversibility and low current, indicating that less NH<sub>4</sub><sup>+</sup> could be oxidated, and part of the oxidated NH<sub>4</sub><sup>+</sup> could be regenerated into NH<sub>4</sub><sup>+</sup> during electrochemical cycles. Hence, the rGO is suitable for applying in ammonium-ion batteries as conductive and blocking layers.

### Author contributions

Huaxia Chen: Design and complete experiments, Process experiment data, Draw the figure, Write the manuscript. Haixin He: Conduct SEM characterization of materials and analysis. Bomiao Wang: Conduct XRD characterization of materials and analysis. Leiyun Han: Interpretation of



data and results. Jian Ma: Interpretation of data and results. Dianpeng Sui: Writing, editing, and interpretation of data and results. Chongtai Wang and Yingjie Hua: Funding acquisition and Project administration.

### CRediT authorship contribution statement

**Huaxia Chen:** Writing – review & editing, Writing – original draft, Investigation. **Haixin He:** Data curation. **Bomiao Wang:** Data curation. **Leiyun Han:** Formal analysis. **Jian Ma:** Formal analysis. **Dianpeng Sui:** Writing – review & editing. **Chongtai Wang:** Writing – review & editing. **Yingjie Hua:** Writing – review & editing.

### Declaration of Competing Interest

There are no conflicts to declare.

### Data availability

Data will be made available on request.

### Acknowledgements

This work was supported by the Hainan Normal University Student Innovation and Entrepreneurship Open Fund (Banyan Tree Fund) (HSRS21-058).

### Appendix A. Supplementary data

Supplementary data to this article can be found online at <https://doi.org/10.1016/j.apenergy.2023.122067>.

### References

- [1] Choi D, Lim S, Han D. Advanced metal–organic frameworks for aqueous sodium-ion rechargeable batteries. *J Energy Chem* 2021;53:396–406.
- [2] Husmann S, Zarbin AJG, Dryfe RAW. High-performance aqueous rechargeable potassium batteries prepared via interfacial synthesis of a Prussian blue-carbon nanotube composite. *Electrochim Acta* 2020;349:136243.
- [3] Sun X, Duffort V, Mehdi BL, Browning ND, Nazar LF. Investigation of the mechanism of mg insertion in Birnessite in nonaqueous and aqueous rechargeable mg-ion batteries. *Chem Mater* 2016;28:534–42.
- [4] Adil M, Sarkar A, Roy A, Panda MR, Nagendra A, Mitra S. Practical aqueous calcium-ion battery full-cells for future stationary storage. *ACS Appl Mater Interfaces* 2020;12:11489–503.
- [5] Zhu K, Wu T, Sun S, Wen Y, Huang K. Electrode materials for practical rechargeable aqueous Zn-ion batteries: challenges and opportunities. *ChemElectroChem*. 2020;7:2714–34.
- [6] Meng J, Song Y, Qin Z, Wang Z, Mu X, Wang J, et al. Cobalt–nickel double hydroxide toward mild aqueous zinc-ion batteries. *Adv Funct Mater* 2022;32:2204026.
- [7] Wang Z, Song Y, Wang J, Lin Y, Meng J, Cui W, et al. Vanadium oxides with amorphous-crystalline heterointerface network for aqueous zinc-ion batteries. *Angew Chem Int Ed* 2023;62:e202216290.
- [8] Cai Y, Chua R, Srinivasan M. Anode materials for rechargeable aqueous Al-Ion batteries: progress and prospects. *ChemNanoMat*. 2022;8:1–17.
- [9] Wu X, Qi Y, Hong JJ, Li Z, Hernandez AS, Ji X. Rocking-chair ammonium-ion battery: a highly reversible aqueous energy storage system. *Angew Chem Int Ed* 2017;56:13026–30.
- [10] Song Y, Pan Q, Lv H, Yang D, Qin Z, Zhang MY, et al. Ammonium-ion storage using electrodeposited manganese oxides. *Angew Chem Int Ed* 2021;60:5718–22.
- [11] Zhang R, Wang S, Chou S, Jin H. Research development on aqueous ammonium-ion batteries. *Adv Funct Mater* 2022;32:2112179.
- [12] Wessells CD, Peddada SV, McDowell MT, Huggins RA, Cui Y. The effect of insertion species on nanostructured open framework Hexacyanoferrate battery electrodes. *J Electrochem Soc* 2011;159:A98–103.
- [13] Lukatskaya MR, Mashtalir O, Ren CE, Dall'Agnese Y, Rozier P, Taberna PL, et al. Cation intercalation and high volumetric capacitance of two-dimensional titanium carbide. *Science*. 2013;341:1502–5.
- [14] Li H, Yang J, Cheng J, He T, Wang B. Flexible aqueous ammonium-ion full cell with high rate capability and long cycle life. *Nano Energy* 2020;68:104369.
- [15] Holoubek JJ, Jiang H, Leonard D, Qi Y, Bustamante GC, Ji X. Amorphous titanic acid electrode: its electrochemical storage of ammonium in a new water-in-salt electrolyte. *Chem Commun* 2018;54:9805–8.
- [16] Xing L, Chen H, Wen X, Zhou W, Xiang K. High performance of co-doped V<sub>2</sub>O<sub>5</sub> cathode material in V<sub>2</sub>O<sub>5</sub>-saturated (NH<sub>4</sub>)<sub>2</sub>SO<sub>4</sub> electrolyte for ammonium ion battery. *J Alloys Compd* 2022;925:166652.
- [17] Liang G, Wang Y, Huang Z, Mo F, Li X, Yang Q, et al. Initiating hexagonal MoO<sub>3</sub> for superb-stable and fast NH<sub>4</sub><sup>+</sup> storage based on hydrogen bond chemistry. *Adv Mater* 2020;32:1907802.
- [18] Zhang N, Cheng F, Liu Y, Zhao Q, Lei K, Chen C, et al. Cation-deficient spinel ZnMn<sub>2</sub>O<sub>4</sub> cathode in Zn(CF<sub>3</sub>SO<sub>3</sub>)<sub>2</sub> electrolyte for rechargeable aqueous Zn-Ion battery. *J Am Chem Soc* 2016;138:12894–901.
- [19] Liu W, Zhang X, Huang Y, Jiang B, Chang Z, Xu C, et al.  $\beta$ -MnO<sub>2</sub> with proton conversion mechanism in rechargeable zinc ion battery. *J Energy Chem* 2021;56:365–73.
- [20] Wang Z, Qin Q, Xu W, Yan J, Wu Y. Long cyclic life in manganese oxide-based electrodes. *ACS Appl Mater Interfaces* 2016;8:18078–88.
- [21] Schweitzer GK, Pesterfiel LL. The aqueous chemistry of the elements. Oxford University Press; 2010.
- [22] Kim KW, Kim YJ, Kim IT, Park GI, Lee EH. Electrochemical conversion characteristics of ammonia to nitrogen. *Water Res* 2006;40:1431–41.
- [23] Zheng R, Li Y, Yu H, Zhang X, Yang D, Yan L, et al. Ammonium ion batteries: material, electrochemistry and strategy. *Angew Chem Int Ed* 2023;62:e202301629.
- [24] Taberna PL, Simon P, Fauvarque JF. Electrochemical characteristics and impedance spectroscopy studies of carbon-carbon supercapacitors. *J Electrochem Soc* 2003;150:A292.
- [25] Akbarinezhad E, Faridi HR. Different approaches in evaluating organic paint coatings with electrochemical impedance spectroscopy. *Surf Eng* 2013;24:280–6.
- [26] Werna J, Turunen I, Salmi T, Maunula T. Kinetics of nitrate reduction in monolith reactor. *Chem Eng Sci* 1994;49:5763–73.
- [27] Vooy AcAd, Santen Rav, Veen JaRv. Electrocatalytic reduction of NO<sub>3</sub><sup>−</sup> on palladiumcopper electrodes. *J Mol Catal A Chem* 2000;154:203–15.
- [28] Kim K-W, Kim Y-J, Kim I-T, Park G-I, Lee E-H. The electrolytic decomposition mechanism of ammonia to nitrogen at an IrO<sub>2</sub> anode. *Electrochim Acta* 2005;50:4356–64.